Control Method Based on Demand Response Needs of Isolated Bus Regulation with Series-Resonant Converters for Residential Photovoltaic Systems

Shu-Huai Zhang [1,†], Feng-Zhang Luo [1,*,†], Yi-Feng Wang [1,†], Jiang-Hua Liu [2,†], Yong-Peng He [2,†] and Yue Dong [2,†]

[1] Key Laboratory of Smart Grid of Ministry of Education, Tianjin University, Tianjin 300072, China; zhangshuhuai@tju.edu.cn (S.-H.Z.); wayif@tju.edu.cn (Y.-F.W.)
[2] Tianjin Research Institute of Electric Science Co., Ltd. (TRIED), Tianjin 300301, China; liujianghua@tried.com.cn (J.-H.L.); hyp_p2006@126.com (Y.-P.H.); dongyue@tried.com.cn (Y.D.)
* Correspondence: luofengzhang@tju.edu.cn; Tel.: +86-139-2090-2432
† These authors contributed equally to this work.

Abstract: Considering the effects of isolation and high efficiency, a series-resonant DC-DC converter (L-L-C type, with two inductors and a capacitor) has been introduced into a residential photovoltaic (PV) generation and storage system in this work, and a voltage gain curve upwarp drifting problem was found. In this paper, the reason of upwarp drifting in the voltage gain curve is given, and a new changing topological control method to solve the voltage regulation problem under light load conditions is proposed. Firstly, the ideal and actual first harmonic approximation (FHA) models are given, and this drifting problem is ascribed to the multiple peaks of higher-order resonance between resonant tank and parasitic capacitors. Then the paper presents the pulse-frequency-modulation (PFM) driver signals control method to translate the full-bridge LLC into a half-bridge LLC converter, and with this method the voltage gain could easily be reduced by half. Based on this method, the whole voltage and resonant current sharing control methods in on-line and off-line mode are proposed. The parameters design and optimization methods are also discussed in detail. Finally, a residential PV system platform based on the proposed parallel 7-kW full-bridge LLC converter is built to verify the proposed control method and theoretical analysis.

Keywords: full-bridge series-resonant converter; light load; parasitic parameters; high order resonant; residential photovoltaic system

1. Introduction

The utilization of residential photovoltaic (PV) power systems, which provide unique advantages of flexible structures and minimal environmental pollution, has become a significant trend in renewable energy applications [1–3]. Because of parasitic capacitance between the PV panels and ground, addressing leakage current and meeting safety requirements are major operating concerns [4,5]. Therefore, electrical isolation of residential PV systems is currently recommended [6–8]. Additionally, in order to make the most of PV power, high-efficiency performance is expected as well. Among potential alternative isolated DC-DC converters, the series-resonant DC-DC converter with resonant inductor, resonant capacitor and magnetizing inductor (we call it LLC resonant converter or LLC below), which has been investigated to improve power conversion efficiency, has attracted interest recently [9–13]. When the working frequency is above the main resonant frequency, LLC can attain zero-voltage-switching (ZVS) for primary power switches. When the working frequency

is below the main resonant frequency, LLC can both attain ZVS for primary power switches and zero-current-switching (ZCS) for output rectifiers [14]. Additionally, the converter benefits from a narrow switching frequency range with light load and ZVS capability, even with no load [15–19].

The comparative study between the LLC resonant converter and three other isolated DC-DC converters was discussed in [20]. It is obvious that LLC has higher efficiency and less volume under the same operating conditions. However, LLC resonant DC-DC converters have several problems, as follows: (1) High voltage gain beyond regulation under light load conditions, as noted in [21]. The traditional way to solve this problem is by adopting burst mode control. Many studies on this approach have been performed. Nevertheless, in the burst mode, the output voltage ripple will be large, leading to lower efficiency; (2) A more serious problem under light load conditions is the upwarp drift of the gain curve. In [22], four factors are introduced in the first harmonic approximation (FHA) model to describe this phenomenon: metallic oxide semiconductor field effect transistor (MOSFET) output capacitance, transformer wiring capacitance, leakage inductance at the transformer secondary side, and junction capacitance of the rectifier diodes. The conclusion drawn is that the junction capacitances of the rectifier diodes are the most influential factor. On the basis of this analysis, the author proposed a method by adding parallel capacitors on the primary side. However, during experimental verification we found that the effect of this method is unsatisfactory. On the other hand, pulse width modulation (PWM) control can be adopted under light load conditions [23], but the exchange between PWM and pulse frequency modulation (PFM) is complicated, and the turn-off current will be larger; (3) In addition, because of the limited bandwidth, the dynamic performance of LLC converters is unfavorable [24]. Different control strategies for LLC resonant converters have been discussed. They are classified as variable-frequency operations and constant-frequency operations [25–27]. Recently, several improved control schemes have been proposed. A mixed control strategy in a neighborhood electric vehicle (NEV) application was proposed [28]. By combining several control strategies, both low-frequency and high-frequency current ripples on the battery are minimized while stability is maintained. Optimal trajectory control based on state-plane analysis can provide very fast dynamic performance for series resonant converters [29]. Also, a Bang-Bang charge control for LLC was proposed [24]. It is simple because it uses only the series resonant capacitor voltage and a pair of voltage thresholds to determine the MOSFETs' switching points. It can achieve high-loop bandwidth and provide fast dynamic performance.

In this study, firstly in Section 2, we describe an existing residential PV power system, and analyze the voltage regulation problem of a parallel full-bridge LLC converter in this system. In Section 3, we discuss the ideal and actual FHA model based on previous research, and aim to analyze the reason of the upwarp drifting in the voltage gain curve. Then, in Section 4, a new changing topological control method to solve the voltage regulation problem at light load condition is proposed. By adapting PFM driver signals, the full-bridge LLC converter can be changed into half-bridge LLC, and the voltage gain could be reduced by half easily for voltage regulation. Design consideration based on the new method is also given in this section. Based on this method, the whole voltage control methods and simulation verifications in on-line and off-line mode are proposed in Section 5. Finally, in Section 6, experimental results with resistive load and real household load are discussed to verify the availability of the proposed control methods.

2. A Residential PV Power System and Problem Description

2.1. System Description

Figure 1 shows the architecture of a residential PV power system, which is composed of four parts. The boost maximum power point tracking (MPPT) converter and the bidirectional DC-DC converter transfer the energy from the PV and batteries to the 400 V DC bus. Compared to the systems placing batteries at the output of PV MPPT converter, the structure in this paper can easily control

charging/discharging state and current of batteries with bidirectional DC/DC converter, which is benefit for the life time and usage cost of the batteries.

Following them, a parallel full-bridge LLC converter is connected to the next 630 V DC bus, which are used to supply high-frequency isolation and voltage regulation for the system. LLC converters guarantee electrical isolation with high working frequency. As its full-load efficiency is 98.4% and maximum efficiency is 98.7% in experiments, efficiency is not reduced largely when energy is transferred from PV and batteries to grid. At the end, a three-phase inverter is connected to the grid, which supplies the household load. The proposed residential PV power system can be operated in both on-line and off-line mode:

(1) In on-line mode, the LLC converters control the 400 V DC bus voltage. The inverter regulates the 630 V DC bus and harmonics of the output currents. The boost converter adopts the MPPT algorithm. The bidirectional converter adopts current control to compensate the power difference between household load and PV.

(2) In off-line mode, the LLC resonant converters control the 630 V DC bus voltage. The inverter regulates the AC output voltage. The boost converter adopts the MPPT algorithm and the bidirectional converter adopts voltage control to regulate the 400 V DC bus voltage.
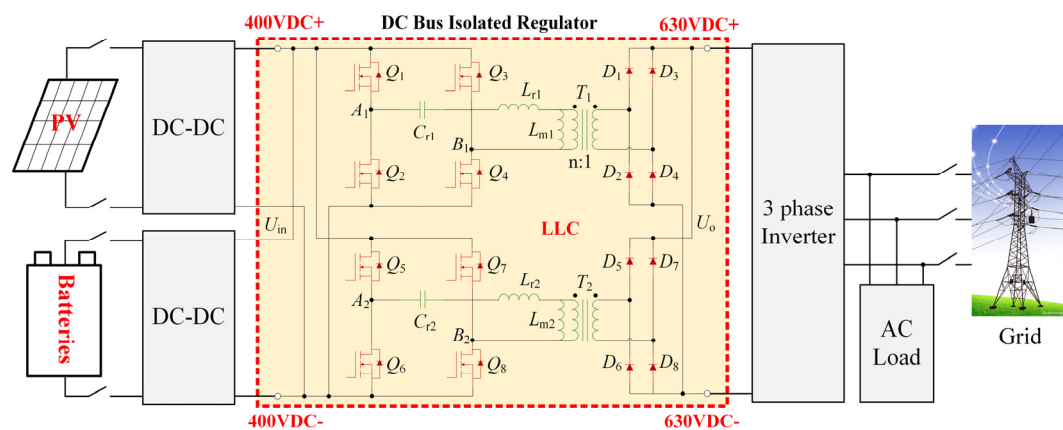

Figure 1. Architecture of residential photovoltaic system.

2.2. Existing Problem Description

In the proposed residential PV system, the energy generated by PV is delivered to the batteries, little power is transmitted to inverter through the LLC resonant DC-DC converters, when the household load is light. The LLC converters may always work at light load condition. So the problem of the upturn of the LLC voltage gain at high frequencies given in [21] will be inescapable. According to experiments, the light load gain is so high that the required voltage (630 V DC or 400 V DC) cannot be restrained. Thus, the voltage regulation problem could be described as following:

(1) In on-line mode, the 400 V DC bus voltage, U_{400}, will be lower than 400 V, and a steady-state error exists, as the 630 V DC bus voltage is constant and regulated by the following inverter with closed-loop control.

(2) In off-line mode, the 630 V DC bus voltage, U_{630}, will be higher than 630 V normally. Burst mode is adopted, too large voltage ripple exists, as the 400 V DC bus voltage is stable and controlled by the bidirectional DC-DC converter, as shown in Figure 1.

(3) Too slow voltage regulation when the load changes, and too large a voltage spike or sink when the load is changing suddenly.

3. Ideal and Actual FHA Model

FHA modeling method is widely used due to its simple and effectiveness. In this paper, FHA modeling process is based on previous research [30,31] and we just used it to analyze and explain the difference between ideal and actual gain of the LLC converter.

Figure 1 shows the topology of the proposed full-bridge LLC resonant converter. The input voltage is U_{in}, the output voltage is U_o. The resonant tank is formed by the resonant capacitor C_r, the resonant inductor L_r and the magnetizing inductor L_m of the transformer. The turn ratio of the transformer is n:1. The switches on the primary side of the transformer (Q_1, Q_2, ... , and Q_8) are MOSFETs. In the output rectifier, D_1, D_2, ... , and D_8 are the rectifier diodes. The DC voltage gain in this paper refers to the ratio of output voltage: U_o/U_{in}.

3.1. Ideal FHA Model Analysis

Firstly, several assumptions are made here:

(1) Waveforms in resonant tank are perfect sinusoidal waves under any working frequency.
(2) All the energy is conveyed by the fundamental component of the input voltage: $u_{in,FHA}$.
(3) All the parasitic parameters are neglected.
(4) Figure 2 shows the ideal equivalent circuit of the proposed full-bridge LLC converter using the FHA modeling method [31].
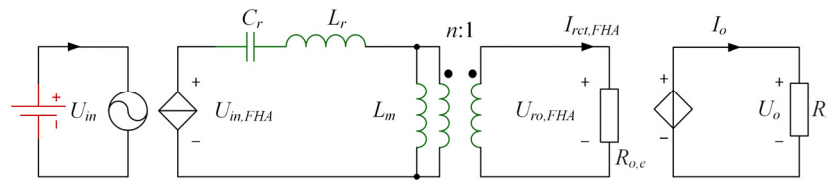

Figure 2. Ideal equivalent circuit of LLC resonant converter

As is known, LLC converter has two resonant frequencies, in this paper we define the higher resonant frequency f_{r1} as the main resonant frequency f_r, that means: $f_r = f_{r1}$. f_{r2} is the secondary or lower resonant frequency:

$$f_{r1} = \frac{1}{2\pi\sqrt{L_rC_r}} \, , \, f_{r2} = \frac{1}{2\pi\sqrt{(L_r + L_m)C_r}} \tag{1}$$

and u_{in} can be expressed with the Fourier series as:

$$u_{in}(t) = \frac{4U_{in}}{\pi} \cdot \sum_{N=1,3,5,\cdots}^{\infty} \frac{1}{N} \sin(2\pi N f t) \tag{2}$$

t is the time parameter, N is the integer parameter for the Fourier series expansion, and f is the switching frequency. According to the above assumptions, the input voltage of LLC resonant network can be regarded as its fundamental component, thus the fundamental component of u_{in} is:

$$u_{in,FHA}(t) = \frac{4U_{in}}{\pi} \cdot \sin(2\pi f t) \tag{3}$$

The root mean square (RMS) value of $u_{in,FHA}$ can be calculated as:

$$U_{in,FHA}(t) = \frac{2\sqrt{2}U_{in}}{\pi} \tag{4}$$

Likewise, the output voltage of the resonant network, can be expressed as:

$$u_{ro}(t) = \frac{4U_o}{\pi} \cdot \sum_{N=1,3,5,\cdots}^{\infty} \frac{1}{N} \sin(2\pi N f t - \phi) \tag{5}$$

where φ is the time shift compared to the input voltage, and the fundamental component of u_{ro} is shown as:

$$u_{ro,FHA}(t) = \frac{4U_o}{\pi} \cdot \sin(2\pi f t - \phi) \tag{6}$$

The RMS value of $u_{ro,FHA}$ can be calculated as:

$$U_{ro,FHA} = \frac{2\sqrt{2}U_o}{\pi} \tag{7}$$

The fundamental component of the rectifier current i_{rct} can be expressed as:

$$i_{rct,FHA} = \sqrt{2}I_{rct,FHA} \sin(2\pi f t - \phi) \tag{8}$$

where $I_{rct,FHA}$ is the RMS value of $i_{rct,FHA}$.

Thus the average output current I_o can be obtained:

$$I_o = \frac{2}{T_s} \int_0^{\frac{T}{2}} |i_{rct,FHA}(t)| \, dt = \frac{2\sqrt{2}}{\pi} I_{rct,FHA} \tag{9}$$

and the equivalent output resistance of the resonant network can be expressed as follows:

$$R_{o,e} = \frac{U_{ro,FHA}}{I_{rct,FHA}} = \frac{\frac{2\sqrt{2}}{\pi}U_o}{\frac{\pi}{2\sqrt{2}}I_o} = \frac{8}{\pi^2}R_o \tag{10}$$

In order to simplify the calculation, the equivalent output resistance in the secondary side of the transformer can be converted to the primary side:

$$R'_{o,e} = n^2 R_{o,e} \tag{11}$$

With all the given parameters, ϕ can be calculated as:

$$\phi = \arctan \left[\frac{2\pi f L_m n^4 R_{o,e}{}^2 + (2\pi f L_r - \frac{1}{2\pi f C_r})(n^4 R_{o,e}{}^2 + 4\pi^2 f^2 L_m{}^2)}{4\pi^2 f^2 L_m{}^2 n^2 R_{o,e}} \right] \tag{12}$$

The forward transfer function of the resonant network can be derived as follows:

$$H(s) = \frac{U_{o,FHA}(s)}{U_{in,FHA}(s)} = \frac{s L_m \cdot R'_{o,e}}{n\left[(s L_m + R'_{o,e})\left(s L_r + \frac{1}{s C_r}\right) + s L_m \cdot R'_{o,e}\right]} \tag{13}$$

Finally, the ideal voltage gain of the LLC resonant converter can be calculated as:

$$\begin{aligned}
G_{id} &= \frac{U_o}{U_{in}} = \frac{U_{o,FHA}}{U_{in,FHA}} = \|H(j2\pi f)\| \\
&= \frac{(j2\pi f)^2 L_m C_r R'_{o,e}}{n\sqrt{\left(R'_{o,e} - (j2\pi f)^2 L_r C_r R'_{o,e} - (j2\pi f)^2 L_m C_r R'_{o,e}\right)^2 + \left((j2\pi f) L_m - (j2\pi f)^3 L_m L_r C_r\right)^2}}
\end{aligned} \tag{14}$$

3.2. Actual FHA Model Analysis Including Parasitic Capacitors

In order to illustrate the upwarp drifting of the voltage gain curve, the junction capacitances of the rectifier diodes and the wiring capacitance of the transformer are added. Its equivalent FHA circuit is shown in Figure 3. C_{pc} represents the total parasitic capacitances of the rectifier diodes and transformer windings. C_{r_PC} represents parasitic capacitance of resonant inductor, which has not been considered

in former work [21]. In our LLC converter, C_{r_PC} = 0.2 nF. C_{r_PC} is so small, and the impact of the parameter of C_{r_PC} can be neglected, so the parameter will not appear in the actual FHA model and analysis in the whole article. From Figure 3, it can be obtained that the reason of the upwarp drifting should be ascribed to the high order resonance between the resonant tank and parasitic capacitors C_{pc}.
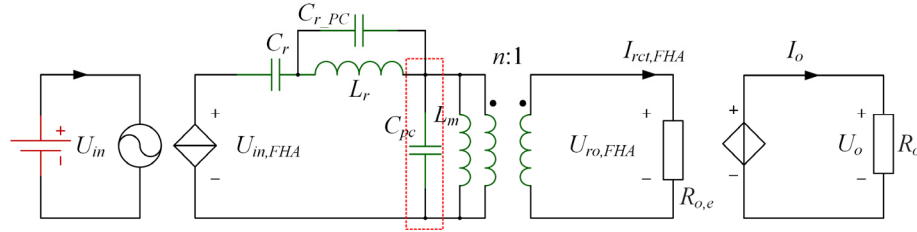

Figure 3. Equivalent model of LLC resonant converter considering parasitic parameters.

After considering C_{pc}, the voltage gain of LLC converter can be rewritten as:

$$G_{pc} = \frac{R'_{o,e} \cdot 2\pi f \cdot C_r \cdot B(f)}{n\sqrt{[A(f) \cdot B(f)]^2 + \{R'_{o,e}[A(f) \cdot 2\pi f \cdot C_{pc} + B(f) \cdot 2\pi f \cdot C_r]\}^2}} \tag{15}$$

where $A(f)$ and $B(f)$ are defined as:

$$A(f) = 4\pi^2 f^2 L_r C_r - 1 \tag{16}$$

$$B(f) = 4\pi^2 f^2 L_m C_{pc} - 1 \tag{17}$$

As shown in Figure 4, the full line is the gain curve considering parasitic parameters with (15), the dash line is the ideal gain curve. The straight dot dashed line is the expected voltage gain (630 V DC/400 V DC = 1.575). Those curves are given under the same output resistance (5 kΩ), and f_r is 78.8 kHz. Therefore, the expected voltage gain cannot be obtained under the model considering actual parasitic parameters, which is the same as the experimental result.
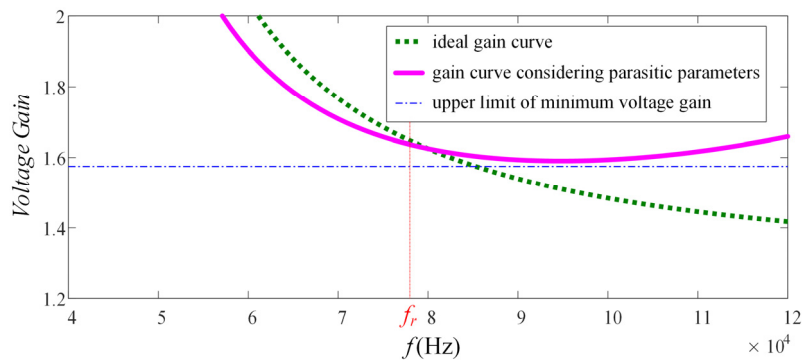

Figure 4. Voltage gain curve of full-bridge LLC converter at light load condition.

4. New Control Method at Light Load Conditions

As shown in Figure 3, there is an additional C_{pc} in the actual FHA model, which is parallel with the transformer. Therefore, the reason of upwarp drifting of the voltage gain curve can be ascribed to the higher-order resonance between resonant tank and parasitic capacitors, and there is an additional resonant bottom where the frequency is higher than the main resonant frequency f_r in Figure 4. But it is hard to calculate the real value of C_{pc} due to the uncertainty of parasitic parameters.

In order to solve this non-monotonic problem simply and effectively, this paper presents a changing topological control method. By adapting PFM driver signals, the full-bridge LLC converter can be changed into half-bridge LLC, and the voltage gain could be reduced by half.

4.1. Proposed Changing Topological Control Method

As shown in Figure 5, a full-bridge LLC can be simply transformed into a half-bridge LLC by turning off Q_3 and turning on Q_4 (as shown in Figure 1) incessantly. The input voltage of resonant tank in full-bridge LLC, u_{AB_F}, ranges from U_{in} to $-U_{in}$ in one period, each voltage lasts 50% of the whole period, but that in half-bridge LLC, u_{AB_H}, ranges from U_{in} to 0 in one period, each voltage lasts 50% of the whole period. Thus, the RMS value of fundamental harmonic of u_{AB_F} in full-bridge LLC, U_{AB_F}, can be displayed as:

$$U_{AB\_F} = \frac{\int_0^{1/f} u_{AB\_F} \cdot dt}{1/f} = \frac{2\sqrt{2}}{\pi} U_{in} \tag{18}$$

And the RMS value of fundamental harmonic of u_{AB_H} in half-bridge LLC, U_{AB_H}, can be displayed as:

$$U_{AB\_H} = \frac{\int_0^{1/f} u_{AB\_H} \cdot dt}{1/f} = \frac{\sqrt{2}}{\pi} U_{in} = \frac{1}{2} U_{AB\_F} \tag{19}$$

By adopting (10), (11) and (15), we can conclude that given the same output resistance R_o, the voltage gain of the half-bridge LLC mode G_{H_pc} is half of that of the full-bridge mode:
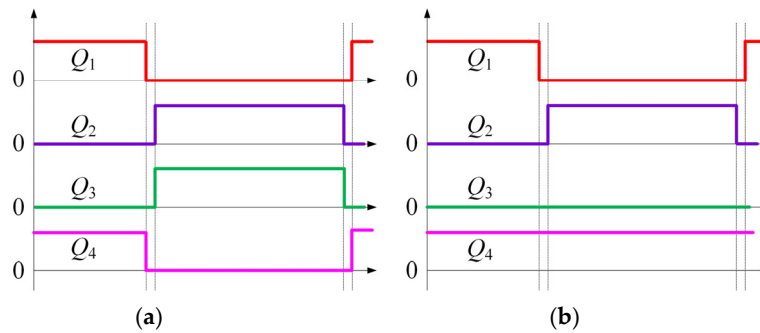
$$G_{H\_pc}(f, R_o) = \frac{1}{2} G_{pc}(f, R_o) \tag{20}$$

Figure 5. Drive signals of the proposed changing topological LLC: (**a**) Full-bridge LLC; and (**b**) Half-bridge LLC.

To verify the above analysis, an open loop experimental based on a half-bridge LLC converter has been carried out. As shown in Figure 6, the solid line is the voltage gain curve calculated by the actual FHA model with (15), and the dashed line is the experimental results, which are obtained by changing the operating frequency under the same input voltage and output resistance (5 kΩ), and f_r is 78.8 kHz. The straight dot dashed line (the same with Figure 4) is the expected voltage gain. Therefore, by utilizing the proposed changing topological control method, the expected voltage gain can be obtained under very light load condition, and even the switching frequency could be reduced.

Compared to the full-bridge LLC, conduction loss and core loss in the half-bridge LLC increases due to the larger RMS of the resonant current. As the switching frequency becomes lower, and MOSFETs in switching mode decrease from 4 to 2, the turn-off loss declines largely. To conclude, at light load condition, the fall of turn-off loss is larger than the rise of conduction loss and core loss. Overall, the efficiency under half-bridge mode is a little higher than that under full-bridge mode.
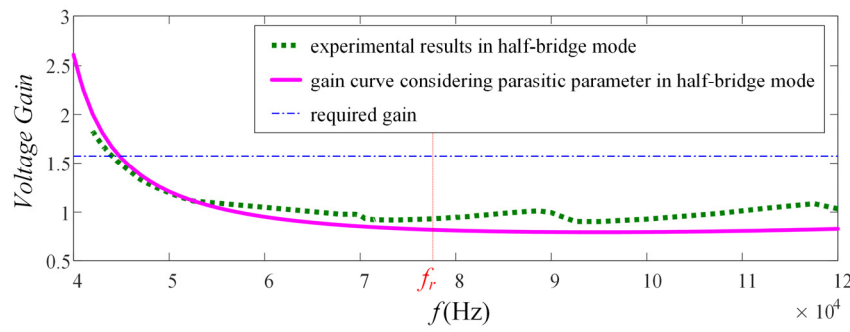
Figure 6. Voltage gain curve of half-bridge LLC.

4.2. Design Consideration Based on the New Method

As is discussed above, to track the required gain of the LLC converter in all load range, it is important to find the required gain in full-bridge mode when load is normal. It is also important to find the required gain in half-bridge mode when load is light, so there are several restrictions. In the following Section 4.2.1, the design procedure of the resonant tank parameters and power devices will be discussed. The requirement and design approach of the voltage gain and working frequency range for the changing topological LLC converter, which are used to meet the voltage gain requirements of the whole load range, will be analyzed in Section 4.2.2.

4.2.1. Resonant Parameters and Rated Operationg Point Design

In this paper, the design procedure of the resonant tank parameters and power devices which is presented in [31] will be adopted. As shown in Figure 7, U_{in_max}, U_{in_min}, U_{out_max} and U_{out_min} are the maximum and minimum of input and output voltage respectively, P_{out_max} is the maximum output power, n, n_p, n_s, L_r, L_m is the turn ratio, turns of primary and secondary, resonant inductor and excitation inductor of the transformer respectively, C_r is the resonant capacitor, C_o is the output filter capacitor, R_{ac} is the effective resistive load reflected to the primary side, G_{max} and G_{min} are the required maximum and minimum voltage gain under full-bridge LLC topology, k is the ratio of L_m to L_r, T_D is the dead-time of the bridge-arms, Q is the quality factor of the resonant tank, f_{max} and f_{min} is the feasible maximum and minimum operating frequency under different load conditions, I_p is the current in the resonant tank, I_m is the excitation current of the transformer, I_{Q_RMS}, U_{Q_max} and P_{Q_max} are the maximum RMS current, drain-source voltage and loss power of each MOSFET respectively, I_{D_avg}, U_{D_max}, P_{D_on} are the maximum average current, inverse voltage and loss power of each rectifier diode respectively, I_{cr_RMS} and U_{Cr_max} are the maximum RMS current and peak resonant voltage of C_r.
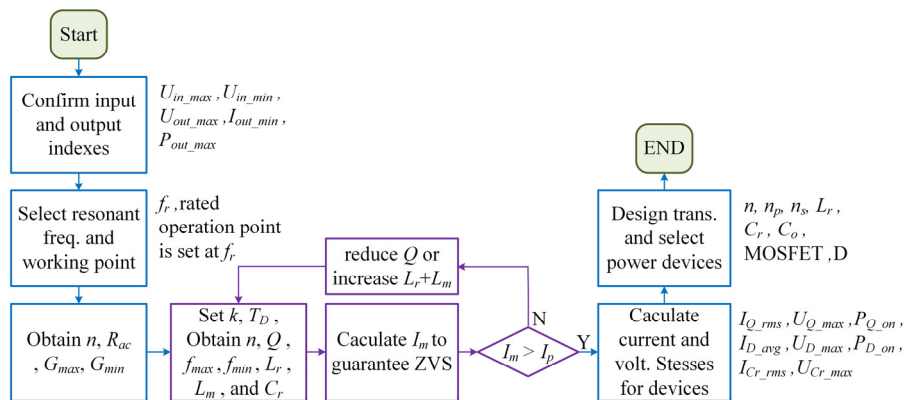

Figure 7. Design procedure of the proposed full-bridge LLC converter.

The design and optimization method is based on full-bridge LLC topology, because the efficiency of normal load range, for example 10–100%, is the main optimization objective and the main operating conditions. On the other hand, the main resonant frequency f_r (or f_{r1}) and rated steady state working frequency are preset. The common setting of f_r is 100 kHz, in this paper, the output power per channel is up to 4 kW, so in order to strike a balance between power efficiency and power density, the setting of f_r will be nearly 80 kHz.

The rated steady state working frequency setting needs to consider the limited peak voltage gain under 4 kW output condition, large DC bus voltage fluctuations caused by the transient procedures and rated conversion efficiency comprehensively.

As the rated power is 4 kW in each channel, it is hard to get a high voltage gain as in [28], because the equivalent resistance R_o is too small to make the curve goes up. Thus, the peak voltage gain should be guaranteed to regulate two DC bus voltage during a large disturbance.

The problem of gain upturn could be avoided by using the proposed changing topological control method, so the limited voltage gain problem should be considered during rated operating point presetting. Therefore, the rated gain can be achieved slightly above the main resonant frequency f_r, making full use of drop scope of gain curve. It can guarantee a wider gain range and higher efficiency near operation point.

4.2.2. Voltage Gain and Working Frequency Range Selection

By using the proposed changing topological control method and the design procedure discussed in Section 4.2.1, the voltage gain and working frequency range selection are illustrated in Figure 8. When the LLC operates in full-bridge LLC mode, $f_{1\text{-}F}$ is the voltage gain peak point under maximum load condition, for example 4.8 kW (1.2 times of rated power), $f_{2\text{-}F}$ is the minimum voltage gain point under selectable minimum load, for example 0.8 kW (0.2 times of rated power). When the load is reduced continuously, the circuit will be changed into half-bridge LLC, $f_{1\text{-}H}$ is the voltage gain peak point under maximum selectable load condition in half-bridge mode, for example 1.2 kW (0.3 times of rated power), $f_{2\text{-}H}$ is the minimum voltage gain point without load. Therefore, within range 2, point 1 is the minimum frequency point and point 2 is the maximum frequency point under full-bridge LLC topology, and within range 1, point 3 is the minimum frequency point and point 4 is the maximum frequency point under half-bridge LLC topology.
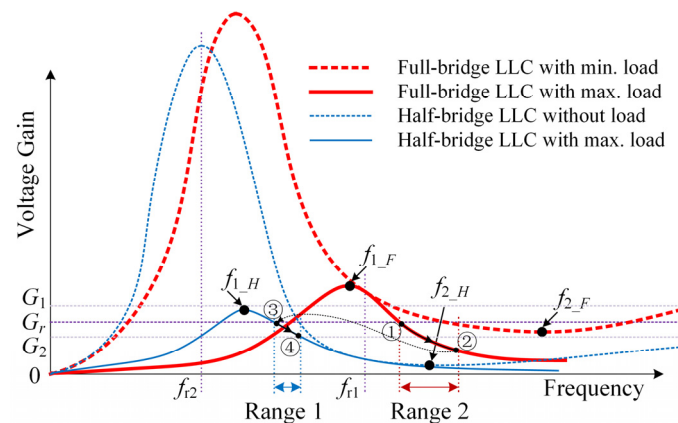

Figure 8. Voltage gain and frequency range selection in full-bridge and half-bridge LLC.

It is necessary to calculate the feasible minimum and maximum frequency, to select the operating frequency range and to ensure a suitable gain can be attained, in which the gain curve is monotonic without upturn.

The first-order derivative of the half-bridge LLC voltage gain can be described as:

$$G'_{H\_pc}(f_{1\_H}, R_o, C_{pc}) = \frac{R'_{o,e} C_r (12\pi^2 f^2 L_m C_{pc} - 1) \cdot \left[C(f)^2 + D(f)^2 \right]}{2n \left[C(f)^2 + D(f)^2 \right]^{\frac{3}{2}}} - \frac{R'_{o,e} C_r \pi f B(f) C(f) \left[6\pi f L_m C_{pc} A(f) + 6\pi f L_r C_r B(f) \right]}{n \left[C(f)^2 + D(f)^2 \right]^{\frac{3}{2}}}$$
$$- \frac{R'^2_{o,e} C_r \pi f B(f) D(f) \left(12\pi^2 f^2 L_r C_r C_{pc} + 12\pi^2 f^2 L_m C_r C_{pc} \right)}{n \left[C(f)^2 + D(f)^2 \right]^{\frac{3}{2}}} + \frac{R'^2_{o,e} C_r \pi f B(f) D(f) (C_{pc} + C_r)}{n \left[C(f)^2 + D(f)^2 \right]^{\frac{3}{2}}} \tag{21}$$

$C(f)$ and $D(f)$ are defined as:

$$C(f) = A(f) \cdot B(f) \tag{22}$$

$$D(f) = 2\pi f \cdot R'_{o,e} \left[C_{pc} \cdot A(f) + C_r \cdot B(f) \right] \tag{23}$$

By making G'_{H_pc} zero, extreme points of G_{H_pc} are obtained. f_{1_H} is a local maximum value point, and f_{2_H} is a local minimum value point. As shown in Figure 8, the frequency range between f_{1_H} and f_{2_H} is the maximum feasible working area for the half-bridge LLC resonant converter, and range 1 should be contained within f_{1_H} and f_{2_H}. Similarly, the frequency range between f_{1_F} and f_{2_F} is the maximum suitable working area for the full-bridge LLC resonant converter, and range 2 should be contained within f_{1_F} and f_{2_F}.

In Figure 8, if G_r declines to the position of G_2, the required gain cannot be tracked with the full-bridge LLC converter. Taking a margin of $0.1G_r$ into consideration, the selection of load or R_o should satisfy the following equation:

$$G_{pc}(f_{2\_F}, R_o, C_{pc}) \le 0.9 G_r \tag{24}$$

The gain of the local maximum point f_{1_F}, should be larger than the required gain. Taking a margin of $0.2G_r$ into consideration:

$$G_{pc}(f_{1\_F}, R_o, C_{pc}) \ge 1.2 G_r \tag{25}$$

In half-bridge mode, the gain of the local maximum point f_{1_H}, should be larger than the required gain G_r. If G_r rises to the position of G_1, the required gain cannot be tracked with the half-bridge LLC converter. Taking a margin of $0.1G_r$ into consideration, the selection of R_o should satisfy the following equation:

$$G_{H\_pc}(f_{1\_H}, R_o, C_{pc}) \ge 1.1 G_r \tag{26}$$

The gain of the local minimum point f_{2_H} should be smaller than the required gain G_r. Taking a margin of $0.2G_r$ into consideration:

$$G_{H\_pc}(f_{2\_H}, R_o, C_{pc}) \le 0.8 G_r \tag{27}$$

Considering the above design method and optimization factors, resonant tank parameters, the voltage gain and frequency range could be calculated.

Furthermore, in order to realize fast dynamic response and good steady performance within the whole load conditions, a new DC bus voltage control and current sharing strategy is proposed for the parallel LLC resonant converter. By ensuring that the LLC works in full-bridge mode with normal load and in half-bridge mode with light load, the DC bus voltage is controllable in all load range. Meanwhile, with a dead-band controller, two resonant inductor currents can be shared evenly. The following Section 5 will discuss the proposed control method under on-line mode and off-line mode separately, and corresponding simulation results will be given.

5. Control of the Variable Structure LLC Converter

As shown in Figure 9, a hysteresis controller is proposed to transform the mode of the proposed LLC converter. P_{inv} is the output power of the inverter, it is equal to the output power of LLC converter when power loss of the inverter is ignored. P_U is the minimum load for the full-bridge LLC converter, and P_L is the maximum load for the half-bridge LLC converter.

If the output power of inverter is above P_U, LLC converter operates in the full-bridge mode. If the output power of inverter is below P_L, LLC converter operates in half-bridge mode. Otherwise,

the mode stays the same. Furthermore, P_L is a little smaller than P_U, in order to avoid continuous power fluctuations around the transition gap.
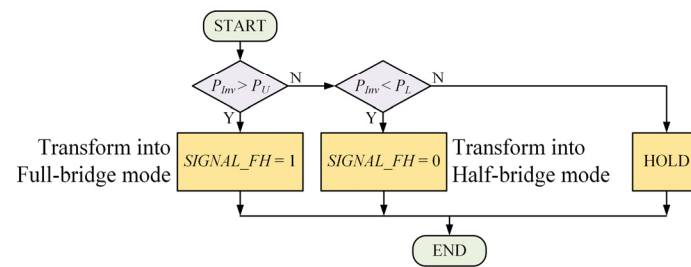

Figure 9. Hysteresis controller for the transform signal generation.

5.1. Proposed Control Scheme in on-Line Mode

As illustrated in Figure 10, U_{400_ref} is the reference of the 400 V DC bus voltage, I_{L1} and I_{L2} are the resonant inductor RMS currents of each channel, f_1 and f_2 are the working frequencies of each channel.

When *SIGNAL_FH* is 0, the converter is transformed into half-bridge mode. The frequency of two LLC resonant converters start to change on the basis of f_{h_on}. Then a dead band controller is used to control the 400 V DC bus voltage. If the 400 V DC bus voltage U_{400} is lower than $(U_{400\_ref} - \Delta U_1)$, the frequencies are increased by Δf_1, to attain lower gain and higher 400 V DC bus voltage. If U_{400} is higher than $(U_{400\_ref} + \Delta U_1)$, the frequencies are altered by Δf_1, to attain higher gain and lower voltage. In this paper Δf_1 is defined as:

$$\Delta f_1 = \begin{cases} -k_1 \cdot \left(U_{400} - U_{400\_ref} \right) & \left| U_{400} - U_{400\_ref} \right| \geq \Delta U_1 \\ 0 & \left| U_{400} - U_{400\_ref} \right| < \Delta U_1 \end{cases} \tag{28}$$

When *SIGNAL_FH* is 1, the gate signals of Q_3 and Q_4 return to normal. The LLC resonant converter operates in full-bridge mode with an initial frequency of f_{f_on}. The controller is similar; the difference is that the step of the dead-band control scheme of DC bus voltage is Δf_2:

$$\Delta f_2 = \begin{cases} -k_2 \cdot \left(U_{400} - U_{400\_ref} \right) & \left| U_{400} - U_{400\_ref} \right| \geq \Delta U_1 \\ 0 & \left| U_{400} - U_{400\_ref} \right| < \Delta U_1 \end{cases} \tag{29}$$

k_1 and k_2 are constant, they are selected by considering the fast response and stability requirements.
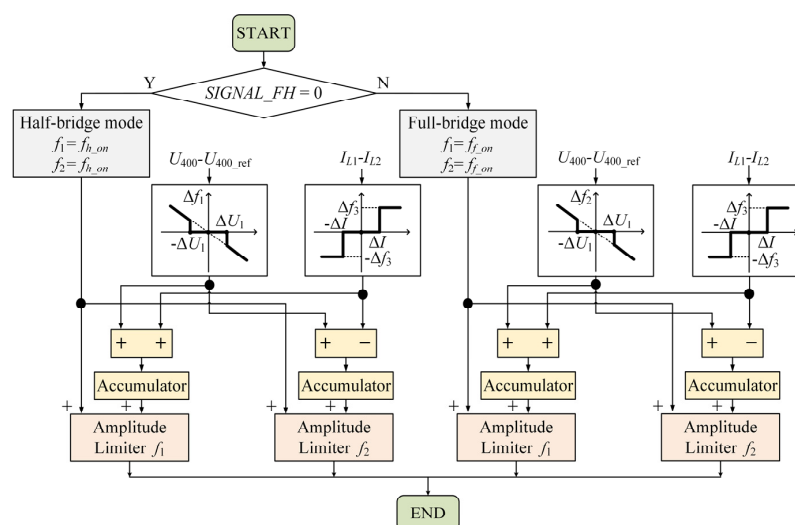

Figure 10. LLC control scheme in on-line mode.

Simultaneously, another dead-band controller works to balance the two LLC currents. In Figure 10, the step of Δf_3 is constant and in fact very small, so the allowable error scope ΔI is $0.02|I_{L1} - I_{L2}|$. If resonant inductor RMS current of first channel LLC is bigger than that of second channel LLC, and the error is over ΔI, working frequency of first channel LLC is increased by Δf_3 and working frequency of second channel LLC is decreased by Δf_3. On the contrary, the working frequency of first channel LLC is decreased by Δf_3 and the working frequency of second channel LLC is increased by Δf_3 Otherwise, when the error between two RMS currents is over $-\Delta I$ and below ΔI, which means two resonant currents are almost balanced, this dead band controller of current sharing doesn't work. By use of fixed step of Δf_3 in dead band controller, resonant currents may not be exactly the same. However, in practical application RMS values of resonant currents need not to be identical. Also, the dead band controller is simple and can make LLC converter more stable.

5.1.1. Transfer Conditions between Half-Bridge and Full-Bridge Mode

Assuming the efficiency of inverter is η, the output voltage of LLC converters is U_{630_ref}, the equivalent output resistance for each LLC, R_P could be expressed as:

$$R_P = \frac{2U^2_{630\_ref} \cdot \eta}{P_{inv}} \tag{30}$$

According to load range selection criteria, to make sure that the transition between half-bridge and full-bridge mode is smooth, the LLC output resistance should satisfy Equations (24)–(27), that means:

$$\begin{cases} \max\{R_{1\_H}, R_{1\_F}\} \leq \frac{2U^2_{630\_ref} \cdot \eta}{P_L} \leq \min\{R_{2\_H}, R_{2\_F}\} \\ \max\{R_{1\_H}, R_{1\_F}\} \leq \frac{2U^2_{630\_ref} \cdot \eta}{P_U} \leq \min\{R_{2\_H}, R_{2\_F}\} \end{cases} \tag{31}$$

where R_{1_F}, R_{1_H} are the minimum solutions to (25) and (26), and R_{2_F}, R_{2_H} are the maximum solution to (24) and (27). The selection of P_L and P_U should meet (31).

5.1.2. Initial Working Frequency Selection

At beginning of each working mode (full-bridge or half-bridge mode), a proper initial operating frequency is necessary to get a smooth transition performance. As is shown in Figure 10, when the converter changes from half-bridge mode to full-bridge mode, the initial frequency f_{f_on} is the solution to the following equation:

$$G_{pc}\left(f_{f\_on}, \frac{2U^2_{630\_ref}}{P_{inv\_rate}}, C_{pc}\right) = G_r \tag{32}$$

P_{inv_rate} is the rated output power of the inverter, and $2(U_{630\_ref})^2/P_{inv\_rate}$ is the corresponding equivalent output resistance of each LLC. When the converter changes from full-bridge mode to half-bridge mode, the initial frequency f_{h_on} could be calculated as:

$$G_{H\_pc}\left(f_{h\_on}, \frac{2U^2_{630\_ref}}{P_L}, C_{pc}\right) = G_r \tag{33}$$

5.2. Simulation Results in On-Line Mode

In order to verify the proposed design scheme, a simulation model is fulfilled in MATLAB. The main simulation parameters are listed in Table 1. To simplify the model and shorten the running time of simulation, only battery is used as source here. To verify the proposed current sharing strategy, the different resonant tank parameters of two channels are given deliberately.

To describe the current sharing result, a parameter named current unbalance factor (CUF) is given, which can be defined as absolute value of error between two resonant RMS currents divided by average value of two resonant RMS currents. CUF = $|2(I_{L1} - I_{L2})/(I_{L1} + I_{L2})|$.

The simulation results in on-line mode are shown in Figure 11. $i_{Battery}$ is the current of battery, i_A is inverter output current of phase A. u_{400}, u_{630} are the same as 400 V DC bus voltage U_{400} and 630

V DC bus voltage U_{630}, but u_{400}, u_{630} represent instantaneous values in this article. According to the control scheme, u_{400} is controlled by LLC converters, and u_{630} is controlled by the inverter.

Table 1. Simulation Parameters.

Parameter	Value
LLC main resonant frequency, f_r	78.8 kHz
LLC secondary resonant frequency, f_{r2}	36.0 kHz
First channel LLC resonant inductor, L_{r1}	60 μH
First channel LLC resonant capacitor, C_{r1}	68 nF
First channel LLC Magnetizing inductor, L_{m1}	228 μH
Second channel LLC resonant inductor, L_{r2}	65 μH
Second channel LLC resonant capacitor, C_{r2}	68 nF
Second channel LLC Magnetizing inductor, L_{m2}	223 μH
400 V DC bus capacitor	200 μF
630 V DC bus capacitor	200 μF
AC bus voltage	380 V (phase to phase)
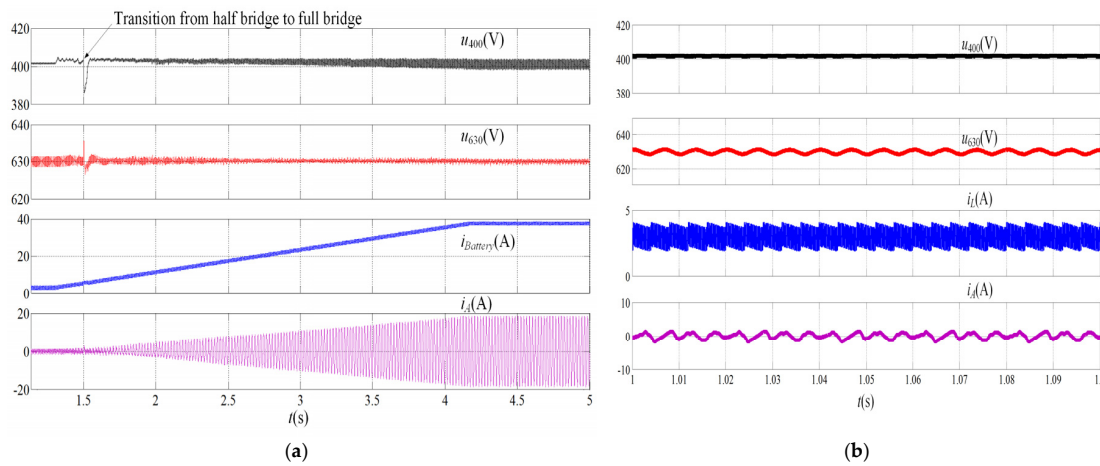
Figure 11. Simulation results in on-line mode: (**a**) transition waveforms; and (**b**) steady state waveforms with light load.

In Figure 11a, the reference of the battery current is 3 A before 1.3 s, and the two LLC resonant converters operate in half-bridge mode. The 400 V DC bus voltage is regulated with no ripple. At 1.3 s, the reference of battery current increases by 12 A/s, so the output currents of the inverter increase accordingly. At 1.5 s, the LLC resonant converters begin to operate in full-bridge mode, and their frequencies are set to f_{f_on}. During this transition, the 400 V DC bus voltage recovers quickly, and the minimum voltage during the transition is 386 V. After approximately 3 s, the reference of the battery current arrives at 37.5 A, and remains unchanged. The entire system is stable and the 400 V DC bus voltage is flat during this period. Figure 11b shows the steady state simulation results at light load condition (half bridge mode), and the 400 V DC bus voltage is stable.

Figure 12 shows the current sharing results of LLC resonant converters with 0 to 7 kW load in on-line mode. At 1.5 s, half-bridge LLC transforms into full-bridge LLC. The figure in inner box shows detailed current waveforms around 2.55 s. It proves that two full-bridge LLC converters work with working frequencies above the main resonant frequency f_r. This is because the required gain is achieved slightly above f_r, making full use of drop scope of gain curve, as the last paragraph in Section 4.2.1 shows. The RMS values of two LLC resonant currents are both 9.6 A in the box, CUF is almost 0. The result indicates that in on-line mode, the proposed current sharing method can balance currents at light and full load condition, even during load transition process.
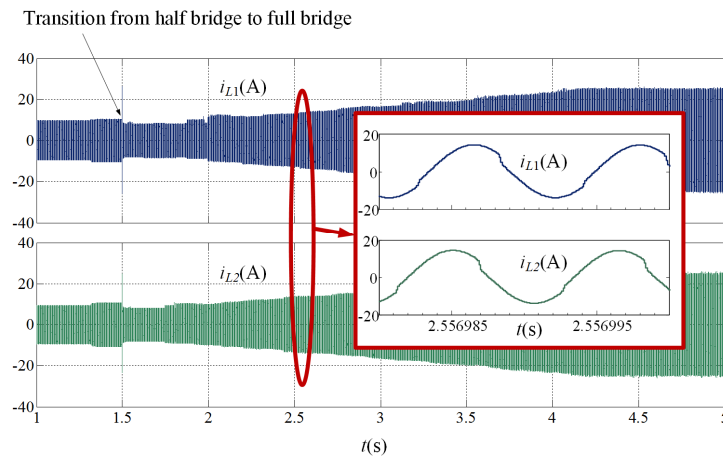
Figure 12. Two channel LLC currents in on-line mode during load transition from 0 to 7 kW load.

5.3. Proposed Control Scheme in Off-Line Mode

In off-line mode, the DC bus voltage control and current sharing strategy of the LLC resonant converter is similar to the strategy in on-line mode, but the DC bus voltage which is controlled by the LLC resonant converters is the 630 V DC bus voltage U_{630}, and the 400 V DC bus voltage U_{400} is controlled by the forestage storage charge and discharge management converter. The architecture in Figure 13 and parameters of the entire simulation model are similar with on-line mode, so the details are not given here repeatedly.
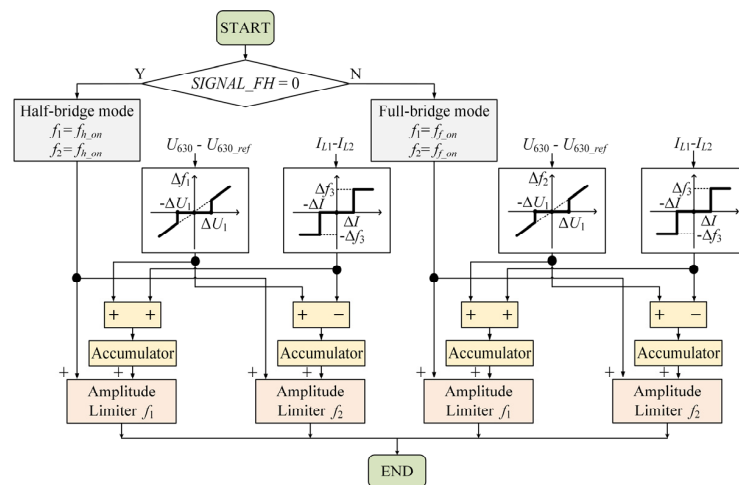
Figure 13. LLC control scheme in off-line mode.

5.4. Simulation Results in Off-Line Mode

In Figure 14a, prior to 1 s, AC load is 50 W, and LLC converter works in half-bridge mode. The 630 V DC bus voltage is regulated with no ripple. At 1 s, the AC load changes to 7 kW, so the LLC resonant converter begins to work in full-bridge mode, and frequency is set initially. During this transition, the 630 V DC bus voltage recovers in 50 ms, the settling time is 24 ms, the minimum voltage during the transition is 586 V, and the maximum voltage is 641 V. The entire system is stable during the transition. Figure 14b shows the simulation results at light load condition (half bridge mode). 630 V DC bus voltage is regulated smoothly.

Figure 15 shows the current sharing results of LLC resonant converters during load transition from 0 to 7 kW in off-line mode. The peak values of two resonant currents are 27.6 A and 27.0 A as

Figure 15 shows. The figure in inner box shows detailed current waveforms around 1.23 s. RMS values of two LLC resonant currents are 11.8 A with 7 kW load. The results indicate that the proposed scheme can divide currents evenly during transition and at full load condition.
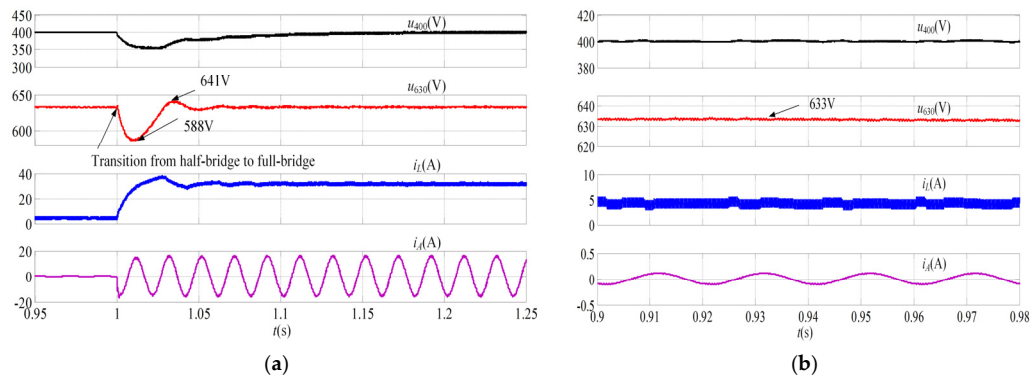

Figure 14. Simulation results in off-line mode: (**a**) transition waveforms; and (**b**) steady state waveforms with light load.
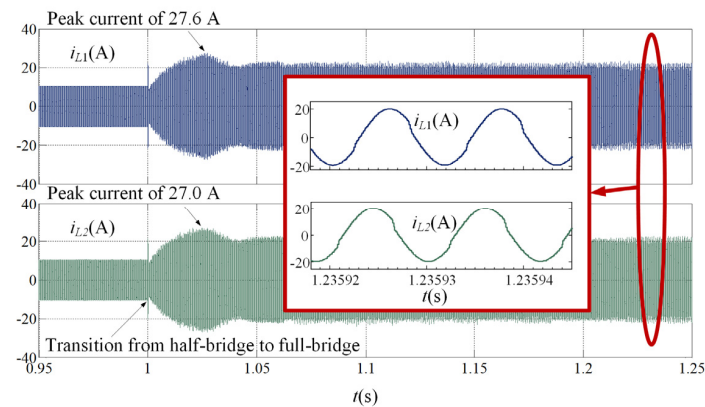

Figure 15. Two channel LLC currents in off-line mode during load transition from 0 to 7 kW.

6. Experimental Results

The proposed control scheme of the full-bridge LLC converters is verified in a 7 kW residential PV system. Figure 16 shows the prototype system.
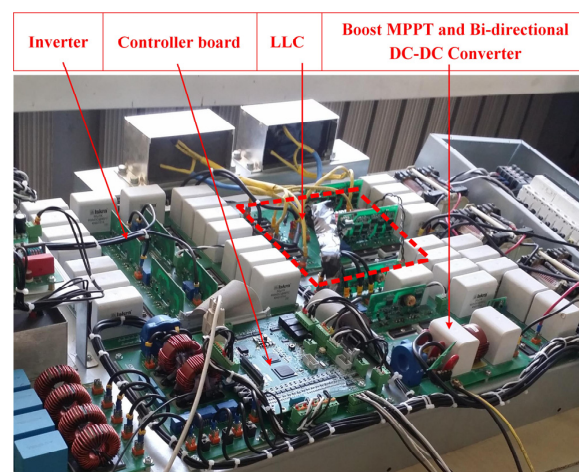
Figure 16. 7 kW residential photovoltaic system hardware setup.

Design criteria and key components are listed in Table 2.

Table 2. Experimental parameters.

Parameter	Value
LLC rated power	4 kW (one channel)
LLC main resonant frequency, f_{r1}	78.8 kHz
LLC secondary resonant frequency, f_{r2}	36.0 kHz
LLC resonant inductor, L_r	60 µH
LLC resonant capacitor, C_r	68 nF
LLC Magnetizing inductor, L_m	228 µH
LLC MOSFET (primary side)	IPW65R045C7 (Infineon, Munich, Germany)
LLC diode rectifier (secondary side)	C4D10120E (Cree, Durhmorning, America)
Battery voltage	100 V DC
PV maximum power	3.5 kW
400 V DC bus capacitor	200 µF
630 V DC bus capacitor	200 µF
AC bus voltage	380 V (phase to phase)
coefficient k_1	12.5 Hz/V
coefficient k_2	62.5 Hz/V
Step3, Δf_3	500 Hz

The PV arrays are replaced by a chroma62150H-1000S programmable DC power supply (Chroma, Taoyuan, Taiwan) with PV simulator. The maximum output power of the PV array simulator is 3.5 kW. The comparison between original waveforms and the optimization waveforms after using proposed control method is also discussed. Furthermore, in order to verify the availability of the proposed control method under real household loads such as air conditioner, microwave and refrigerator, experiments with real household loads are carried out.

6.1. Experimental Results in On-Line Mode

In this mode, the control object is u_{400}. Figure 17 shows the experimental results with the original control method in on-line mode. A steady-state error of -25 V exists in u_{400}. After increasing the load from 0 to 7 kW, there is a pulse of 437 V and fluctuation during transition. The settling time is about 0.35 s. The current balance is out of control during transition process.
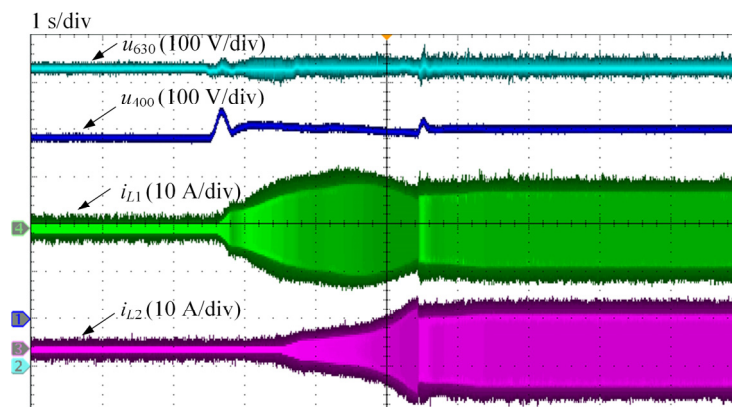

Figure 17. Waveforms of AC load increases from 0 to 7 kW in on-line mode with the original control method.

Figures 18 and 19 show the experimental results with proposed control scheme in on-line mode. In Figure 18, during the transition of the LLC converters from 0 to 7 kW, the fluctuation of 400 V DC

bus voltage is only -14 V, and the settling time can be neglected. The currents of the two LLC resonant inductors are shared evenly at last, with RMS of 12.2 A and 12.0 A. The CUF is about 1.7%.
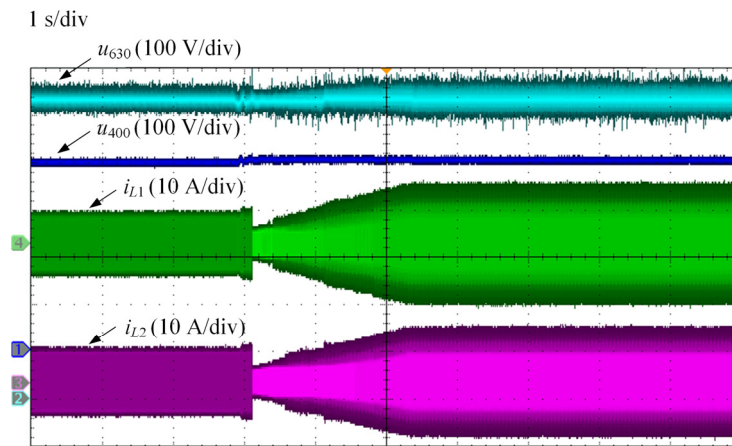

Figure 18. Waveforms of AC load increases from 0 to 7 kW in on-line mode with the original control method.
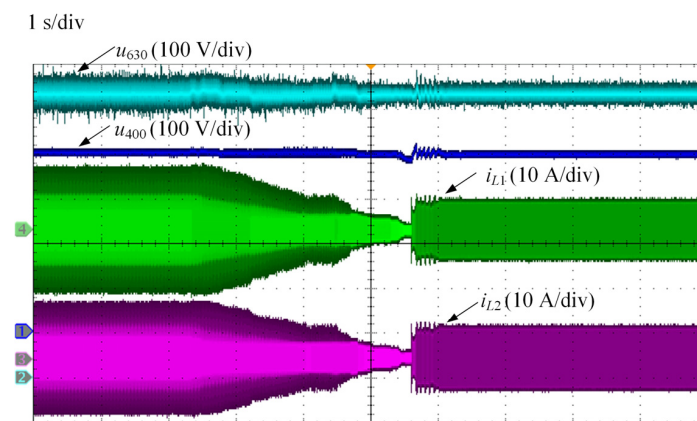

Figure 19. Waveforms of AC load transition from 7 kW to 0 in on-line mode with the new control scheme.

Figure 19 shows a similar result when the AC load decreases from 7 kW to 0. For 400 V DC bus voltage, the maximum voltage drop is 18 V and the peak value is 422 V. What needs illustration is that u_{630} is controlled by inverter and the control method is not optimized. As space is limited, although the fluctuation of u_{630} is a little large, we will not discuss this problem here.

6.2. Experimental Results in Off-Line Mode

In this mode, the control object of LLC is u_{630}. Figure 20 shows experimental results with the original control method in off-line mode. At no load condition, the controller works in burst mode. The voltage ripple is about 50 V, and the peak value is about 693 V. During the transition from 0 to 7 kW, in the worst case, the maximum voltage drop is about 211 V. The settling time is 0.63 s.

Figures 21 and 22 show the experimental results with the proposed control method in off-line mode. As shown in Figure 21, when AC load increases from 0 to 7 kW, with the proposed control scheme, the 630 V DC bus voltage declines to 589 V during the transition and recovers after 21 ms. The peak voltage is 642 V. The maximum CUF is about 0.7%. The experimental results are in consistent with simulation results. Figure 22 shows the experimental waveforms with AC load variation from 7 kW to 2.3 kW to 0. The 630 V DC bus voltage fluctuation is only about 10 V during transition.
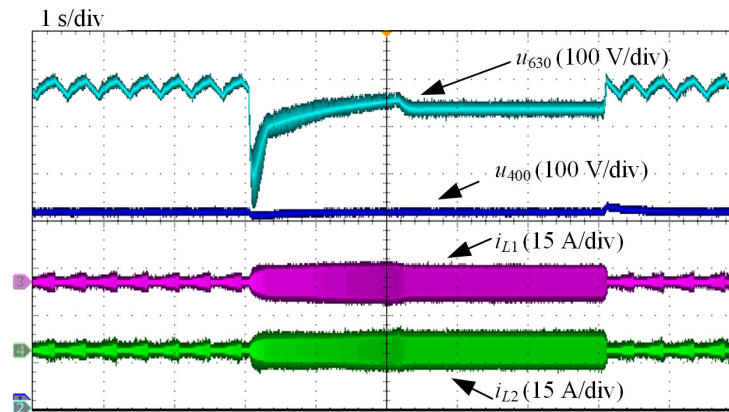
Figure 20. Waveforms of AC load increases from 0 to 7 kW in off-line mode with the original control method.
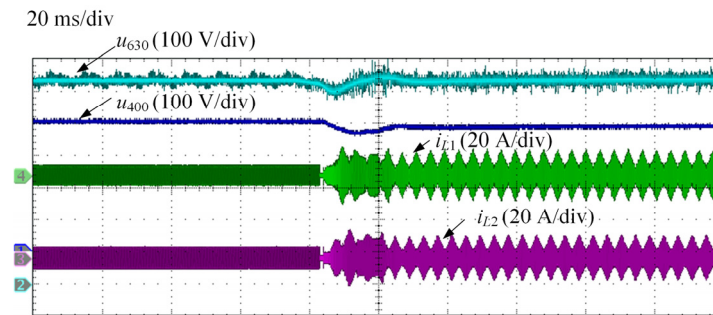

Figure 21. Waveforms of AC load transition from 0 to 7 kW in off-line mode.
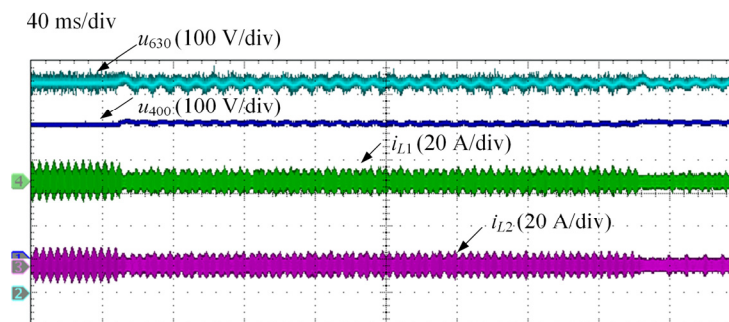

Figure 22. Waveforms of AC load transition from 7 kW to 2.3 kW to 0 in off-line mode.

6.3. Experimental Results with Real Household Load

In order to verify the availability of the improved control method for the residential PV system, experiments are conducted with real household loads. Here the 400 V DC bus voltage and the 630 V DC bus voltage are observed through a real time sampling device, $u_{SIGNAL400}$ represents 400 V DC bus voltage, and $u_{SIGNAL630}$ represents 630 V DC bus voltage.

6.3.1. Experimental Results with Air Conditioner in On-Line Mode

A 4-kW air conditioner is used as an AC load in on-line mode. Figure 23 shows the transient waveforms when the air conditioner is shutdown. During this transition, the currents of LLC and inverter decline slowly, and the LLC converter always works in full-bridge mode. The 400 V and 630 V DC bus voltage are flat and the entire system is stable. Here i_{L1} is current of first channel LLC resonant inductor, and i_A is inverter output current of phase A.
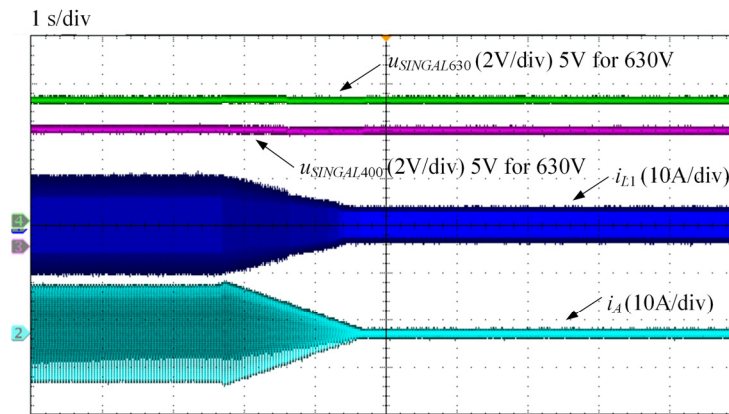
1 s/div

Figure 23. Waveforms when 4 kW air conditioner shutdown in on-line mode.

6.3.2. Experimental Results with Microwave and Refrigerator in Off-Line Mode

In order to verify the impact loading response ability of the proposed control method, a 1.5 kW microwave oven and a 200 W refrigerator are used. Figure 24 shows the waveforms during turning-on operations of the two loads. The 630 V DC bus voltage, phase voltage of inverter and first channel LLC working frequency, are observed through the same real time sampling device. Here $u_{SIGNALA}$ represents phase A voltage, $f_{SIGNALs1}$ represents working frequency of first channel LLC. During this period, LLC transforms from half-bridge to full-bridge mode as its working frequency shows, u_{630} declines to 555 V and recovers after 30 ms, the steady fluctuation is about 60 V. The distorted current is caused by the microwave and refrigerator, which don't have power factor correction ability. The entire system is stable.
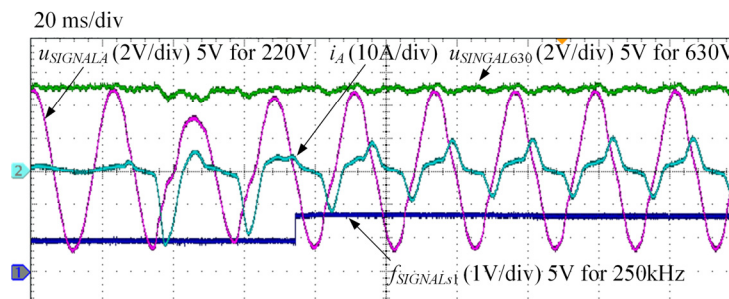
20 ms/div

Figure 24. Waveforms when turn on microwave oven and refrigerator in off-line mode.

7. Conclusions

In this work, a new method to regulate voltage for a full-bridge LLC resonant converter under light load conditions is proposed to solve the voltage gain curve upwarp drift problem. This method transforms a full-bridge LLC resonant converter into a half-bridge LLC resonant converter by adapting PFM driver signals simply. Ideal and actual FHA models are analyzed based on previous reference method. Furthermore, a new voltage and current sharing control scheme in on-line and off-line mode to enhance LLC performance in a residential PV system is implemented. Based on this control scheme, the DC bus voltage is regulated smoothly in all load range, and the two LLC resonant inductor currents are shared well.

Matlab simulation and experimental results, based on resistive load, are performed in the laboratory. In on-line mode, steady-state error of 400 V DC bus voltage is eliminated under light load conditions. During load transition from 0 to 7 kW, the 400 V DC bus voltage has a drop of 14 V in simulation and stays stable in the experiments. The settling time declines from 0.35 s to almost 0 in the experiments. CUF is almost 0 in the simulation and 1.7% in the experiments. In off-line mode,

burst mode is eliminated and ripple is restrained. During load transition from 0 to 7 kW, 630 V DC bus voltage has a drop of 42 V and a rise of 11 V in simulation, while it has a drop of 41 V and a rise of 12 V in the experiments. The settling time declines from 0.63 s to 21 ms in the experiments. CUF is almost 0 in simulation and 0.7% in the experiments. Furthermore, the experimental results have also been carried out with real household loads. The waveforms show that the improved residential PV system can work stably with real household loads such as an air conditioner, microwave oven and refrigerator.

Author Contributions: Shu-Huai Zhang, Feng-Zhang Luo and Yi-Feng Wang proposed the control method, completed theoretical analysis and simulation. Feng-Zhang Luo is also responsible for writing and revising the paper. Jiang-Hua Liu, Yong-Peng He and Yue Dong helped in modifying control algorithm and conducting experiments.

Conflicts of Interest: The authors declare no conflict of interest.

References

1. Kim, Y. Modeling and Analysis of a DC Electrical System and Controllers for Implementation of a Grid-Interactive Building. *Energies* **2017**, *10*, 427. [CrossRef]
2. Jung, S.; Kim, D. Pareto-Efficient Capacity Planning for Residential Photovoltaic Generation and Energy Storage with Demand-Side Load Management. *Energies* **2017**, *10*, 426. [CrossRef]
3. Wang, Y.; Lin, X.; Pedram, M. Adaptive Control for Energy Storage Systems in Households with Photovoltaic Modules. *IEEE Trans. Smart Grid* **2014**, *5*, 992–1001. [CrossRef]
4. Ahmed, T.; Soon, T.; Mekhilef, S. A Single Phase Doubly Grounded Semi-Z-Source Inverter for Photovoltaic (PV) Systems with Maximum Power Point Tracking (MPPT). *Energies* **2014**, *7*, 3618–3641. [CrossRef]
5. Chen, W.; Yang, X.; Zhang, W.; Song, X. Leakage Current Calculation for PV Inverter System Based on a Parasitic Capacitor Model. *IEEE Trans. Power Electron.* **2016**, *31*, 8205–8217. [CrossRef]
6. Tsai, C.; Shen, C.; Su, J. A Power Supply System with ZVS and Current-Doubler Features for Hybrid Renewable Energy Conversion. *Energies* **2013**, *6*, 4859–4878. [CrossRef]
7. Isoda, H.; Kimura, G.; Shioya, M.; Ohsato, M.H. Battery charging characteristics in small scaled photovoltaic system using resonant DC-DC converter with electric isolation. In Proceedings of the International Conference on Industrial Electronics, Control, and Instrumentation (IECON), Pacific Grove, CA, USA, 23–27 November 1990; Volume 2, pp. 1118–1123.
8. Zhan, W.; Li, H. An Integrated Three-Port Bidirectional DC–DC Converter for PV Application on a DC Distribution System. *IEEE Trans. Power Electron.* **2013**, *28*, 4612–4624.
9. Yang, B.; Lee, F.C.; Zhang, A.J.; Huang, G. LLC resonant converter for front end DC/DC conversion. In Proceedings of the Applied Power Electronics Conference and Exposition, Dallas, TX, USA, 10–14 March 2002; Volume 2, pp. 1108–1112.
10. Jin, K.; Ruan, X. Hybrid full-bridge three-level LLC resonant converter—A novel dc-dc converter suitable for fuel cell power system. *IEEE Trans. Ind. Electron.* **2006**, *53*, 1492–1503. [CrossRef]
11. Yang, B.; Chen, R.; Lee, F.C. Integrated magnetic for LLC resonant converter. In Proceedings of the Applied Power Electronics Conference and Exposition, Dallas, TX, USA, 10–14 March 2002; Volume 1, pp. 346–351.
12. Jung, J.; Kim, H.; Ryu, M.; Baek, J. Design methodology of bidirectional CLLC resonant converter for high-frequency isolation of DC distribution systems. *IEEE Trans. Power Electron.* **2013**, *28*, 1741–1755. [CrossRef]
13. Jiang, T.; Zhang, J.; Wu, X.; Sheng, K.; Wang, Y. A Bidirectional LLC Resonant Converter with Automatic Forward and Backward Mode Transition. *IEEE Trans. Power Electron.* **2015**, *30*, 757–770. [CrossRef]
14. Zhang, J.; Liao, J.; Wang, J.; Qian, Z. A current-driving synchronous rectifier for an LLC resonant converter with voltage-doubler rectifier structure. *IEEE Trans. Power Electron.* **2012**, *27*, 1894–1904. [CrossRef]
15. Han, J.H.; Lim, Y.C. Design of an LLC Resonant Converter for Driving Multiple LED Lights Using Current Balancing of Capacitor and Transformer. *Energies* **2015**, *8*, 2125–2144. [CrossRef]
16. Jiang, J.; Pidaparthy, S.K.; Choi, B. Current Mode Control for LLC Series Resonant DC-to-DC Converters. *Energies* **2015**, *8*, 6098–6113. [CrossRef]

17. Cho, S.; Kim, C.; Han, S. High-efficiency and low-cost tightly regulated dual-output LLC resonant converter. *IEEE Trans. Ind. Electron.* **2012**, *59*, 2982–2991. [CrossRef]

18. Hyeon, B.C.; Cho, B.H. Analysis and Design of the LLC Resonant Converter for Low Output Current Ripple. *IEEE Trans. Ind. Electron.* **2012**, *59*, 2772–2780. [CrossRef]

19. Fang, X.; Hu, H.; Shen, Z.J.; Batarseh, I. Operation mode analysis and peak gain approximation of the LLC resonant converter. *IEEE Trans. Power Electron.* **2012**, *27*, 1985–1995. [CrossRef]

20. Yang, B. Topology Investigation of Front-End DC/DC Converter for Distributed Power System. Ph.D. Thesis, Virginia Tech, Blacksburg, VA, USA, September 2003.

21. Kim, J.H.; Kim, C.E.; Kim, J.K.; Moon, G.W. Analysis for LLC resonant converter considering parasitic components at very light load condition. In Proceedings of the 8th International Conference on Power Electronics, Jeju, Korea, 30 May–3 June 2011; pp. 1863–1868.

22. Lee, B.H.; Kim, M.Y.; Kim, C.E.; Park, K.-B.; Moon, G.W. Analysis of LLC resonant converter considering effects of parasitic components. In Proceedings of the INTELEC 31st International Telecommunications Energy Conference, Incheon, Korea, 18–22 October 2009; pp. 1–6.

23. Pan, H.; He, C.; Ajmal, F.; Chen, H.; Chen, G. Pulse-width modulation control strategy for high efficiency LLC resonant converter with light load applications. *IET Power Electron.* **2014**, *7*, 2887–2894. [CrossRef]

24. Hu, Z.; Liu, Y.F.; Sen, P.C. Bang-Bang charge control for LLC resonant converters. *IEEE Trans. Power Electron.* **2015**, *30*, 1093–1108.

25. Kowstubha, P.; Krishnaveni, K.; Reddy, K.R. Review on different control strategies of LLC series resonant converters. In Proceedings of the 2014 International Conference on Advances in Electrical Engineering (ICAEE), Vellore, India, 9–11 January 2014; pp. 1–4.

26. Pahlevaninezhad, M.; Eren, S.; Jain, P.; Bakhshai, A. Self-sustained oscillating control technique for current-driven full-bridge DC/DC converter. *IEEE Trans. Power Electron.* **2013**, *28*, 5293–5310. [CrossRef]

27. Kim, B.C.; Park, K.B.; Moon, G.W. Asymmetric PWM control scheme during hold-up time for LLC resonant converter. *IEEE Trans. Ind. Electron.* **2012**, *59*, 2992–2997. [CrossRef]

28. Musavi, F.; Cracium, M.; Gautam, D.S.; Eberle, W. Control strategies for wide output voltage range LLC resonant DC–DC converters in battery chargers. *IEEE Trans. Veh. Technol.* **2014**, *63*, 1117–1125. [CrossRef]

29. Feng, W.; Lee, F.C.; Mattavelli, P. Optimal trajectory control of burst mode for LLC resonant converter. *IEEE Trans. Power Electron.* **2013**, *28*, 457–466. [CrossRef]

30. Jung, J.H.; Kwon, J.G. Theoretical analysis and optimal design of LLC resonant converter. In Proceedings of the European Conference on Power Electronics and Applications, Aalborg, Denmark, 2–5 September 2007; Volume 1, pp. 1–10.

31. Simone, S.D.; Adragna, C.; Spini, C.; Gattavari, G. Design-oriented steady-state analysis of LLC resonant converters based on FHA. In Proceedings of the International Symposium on Power Electronics, Electrical Drives, Automation and Motion IEEE, Taormina, Italy, 23–26 May 2006; pp. 200–207.